Structure and stability of $NaTaO_3$(001) and $KTaO_3$(001) surfaces

Xunhua Zhao* and Annabella Selloni
Department of Chemistry, Princeton University, Princeton, New Jersey 08540, USA

(Received 9 October 2018; published 2 January 2019)

We carried out first-principles slab calculations to investigate the structure, energetics, and electronic properties of the majority (001) surfaces of $NaTaO_3$ (NTO), a perovskite oxide with excellent photocatalytic properties, and $KTaO_3$ (KTO), a closely related but somewhat less active compound. Being polar, NTO(001) and KTO (001) require charge compensation to be stabilized. We examine a number of possible structural models for these surfaces by comparing their formation energies to those of the pure NaO/KO and TaO_2 terminations. Our results show that a "cation-exchange" reconstruction is energetically most favorable for NTO(001) under vacuum conditions, whereas for KTO(001) this reconstruction competes with a "striped" phase with equally exposed KO and TaO_2 terraces actually observed in recent experiments. NTO is found to exhibit enhanced structural flexibility and more effective charge compensation in comparison to KTO, which is attributed to the significantly smaller size of Na^+ relative to K^+. Upon exposure to water, a (2×1) hydroxylated structure is by far most favorable for both NTO and KTO. This structure can thus provide a basis for the mechanistic understanding of photocatalytic processes on NTO and KTO surfaces.

DOI: 10.1103/PhysRevMaterials.3.015801

I. INTRODUCTION

Perovskite oxides, formally ABO_3, have been extensively studied for their interesting physical properties and their potential use in different areas, such as photocatalysis [1–4], solar cells [5,6], and transistors [7,8]. Of particular interest in photocatalysis and related applications, $NaTaO_3$ and $KTaO_3$ are two representative perovskites [9,10] in which A has a formal charge $+1$, B has charge $+5$, and O is -2. Despite many similarities, $NaTaO_3$ (NTO) and $KTaO_3$ (KTO) exhibit distinct properties. While KTO has a nearly ideal cubic structure, NTO has both a monoclinic (nearly cubic) structure (here denoted c-NTO) and an orthorhombic phase (denoted o-NTO). NTO, especially in its cubic phase, shows extraordinary water-splitting activity, significantly higher than KTO [11–13]. On the other hand, KTO has recently attracted attention for hosting a two-dimensional electron gas at its (001) surface [14], which might be used for novel electronic applications.

As most perovskites, NTO and KTO preferentially expose {001} surfaces, which result from a stacking sequence of alternating AO and TaO_2 (001) planes with formal charges -1 and $+1$ along the [001] direction. While this could in principle lead to a divergence of the electrostatic energy (sometimes called a "polar catastrophe") [15–17] and therefore an instability of the surface as the thickness of the sample increases, in macroscopic samples the dipole is naturally removed by a surface compensation mechanism, such as the formation of defects, the adsorption of molecular species, surface reconstruction [18], and the coexistence of both AO and BO_2 terminations [19,20]. In particular, a computational study based on a global minimum search for surface structures identified a very stable "cation-exchange" reconstruction for KTO(001), where TaO units of the ideal TaO_2-terminated surface descend from the surface into the subsurface layer, while K ions migrate upward from the subsurface into the surface layer [18]. Experimentally, however, a labyrinthlike pattern consisting of equally exposed KO and TaO_2 stripes was recently revealed by atomic force microscopy (AFM) and scanning tunneling microscopy (STM) measurements in vacuum, while a hydroxylated (2×1) reconstruction was observed upon exposure to water [21]. As for NTO, experimental information comes from studies on disperse samples. Regularly spaced nanosteps of 3–15 nm have been observed on doped and high-temperature treated samples [2,22], but the atomic-scale details of the surface structure are still unknown.

In this work, we seek to obtain insight into the surface structure of NTO through a comparative first-principles study of NTO (001) and KTO (001) surfaces and the role of the different Na^+ and K^+ cation sizes [23,24] in their stability. Our results show that the cation-exchange reconstruction [18] is energetically preferred on both the NTO and KTO surfaces in vacuum. For KTO, this structure is computed to be even slightly more stable than a "striped" phase with equally exposed KO and TaO_2 terraces, as observed experimentally [21], suggesting that kinetics also has a role in establishing the surface compensation mechanism. Since NTO is known to have very high activity for photocatalytic water splitting, we also studied the interaction with water, in particular the influence of water on the stability of the different surface structures studied in vacuum. Our results show that upon exposure to water the cation-exchange reconstruction is destabilized because all exposed Ta atoms are saturated, and cannot bind to H_2O. Instead, a hydroxylated (2×1) structure, as

*Present address: Texas Materials Institute and Department of Mechanical Engineering, The University of Texas at Austin, Austin, TX 78712.

observed for KTO [21], is found to be most stable for both NTO(001) and KTO(001) in a humid environment.

II. METHODS AND MODELS

Density functional theory (DFT) calculations were conducted with the QUANTUM ESPRESSO package [25]. The gradient-corrected Perdew-Burke-Ernzerhof (PBE) functional [26] was used together with ultrasoft pseudopotentials [27,28] to represent the core electrons. Valence electrons were described using a plane-wave basis set with cutoffs of 40 and 320 Ry for the electron wave functions and charge density, respectively. With this setup, defect formation energies (see below) were converged to 0.01 eV. Single-point HSE06 hybrid functional calculations were performed using the FHI-AIMS code [29,30] with default "tight" basis.

KTO has a nearly ideal cubic structure; thus the primitive cell contains five atoms, with Ta at the center of an octahedron and K in 12-fold cuboctahedral coordination [Figs. 1(a) and 1(b)]. As in other theoretical studies [31,32], we adopted a cubic model [Figs. 1(a) and 1(b)] also for the NTO monoclinic phase. For the cubic (orthorhombic) cell, a $5 \times 5 \times 5$ ($6 \times 6 \times 3$) k-point mesh was found sufficient to obtain total energies converged to about 1 meV and crystal lattice constants converged to 0.001 Å. The orthorhombic phase, Fig. 1(c), can be considered as a c(2×2) structure with the cubic lattice distorted and the octahedra tilted aside. Bulk defect formation energies were determined using a $(2 \times 2 \times 2)$ supercell for c-NTO and KTO, and a $(\sqrt{2} \times \sqrt{2} \times \sqrt{2})$ supercell for o-NTO (40 atoms). The oxygen vacancy (Vo) formation energy was calculated as $E_{\text{form}} = E_{\text{Vo}} - E_{\text{pristine}} + \frac{1}{2}E_{\text{O}_2}$, where the terms on the right side are the total energies of the supercell with Vo, pristine supercell, and half of the isolated oxygen molecule, respectively.

The NTO and KTO (001) surfaces were studied using a few different slab models. Symmetric, nonstoichiometric slabs were used to study some properties of the NaO(NO)/KO and TaO_2 (TO) terminations separately, while stoichiometric nonsymmetric slabs with NO/KO on one side and TO on the other side were used to investigate polarization effects and determine the surface energies of each termination. In both cases a (1×1) surface unit cell was used. As for the slab thickness, after test calculations, we typically chose a thickness of 6.5 unit cells (u.c.), i.e., 13 atomic layers, for symmetric slabs and 7 u.c. for nonsymmetric ones. A Monkhorst-Pack (MP) mesh [33] of $5 \times 5 \times 1$ k points was used for these slab models. For the nonsymmetric models, dipole corrections were added to remove the field in the vacuum region [34]. Surfaces with alternating and equally exposed NO/KO and TO terraces separated by steps along the [110] direction [21] were investigated using symmetric stoichiometric slab models with $(\sqrt{2} \times w\sqrt{2})$ surface cells, where $w = 2, 3, 4, 5$ represents the width of the terraces; the typical slab thickness was 10 to 12 atomic layers, so that, for example, $w = 3$ corresponds to a slab containing 156 atoms. MP meshes of $5 \times 3 \times 1$, $5 \times 2 \times 1$, $5 \times 1 \times 1$, and $5 \times 1 \times 1$ k points were used for $w = 2, 3, 4$, and 5, respectively. These slabs were optimized by relaxing the positions of all atoms except those in the central TaO_2 layer until the total energy change was smaller than 10^{-4} a.u. and the force on every atom was smaller than 10^{-3} a.u. Reconstructed surfaces were studied based on the model of Ref. [18]. Since experimentally the oxide films are often grown on a metal substrate [35,36], NTO/KTO slabs on a buffer Ta metal substrate were also examined. These slabs were 13 to 14 atomic layers thick, with (1×1) unit cells; the MP mesh was $5 \times 5 \times 1$.

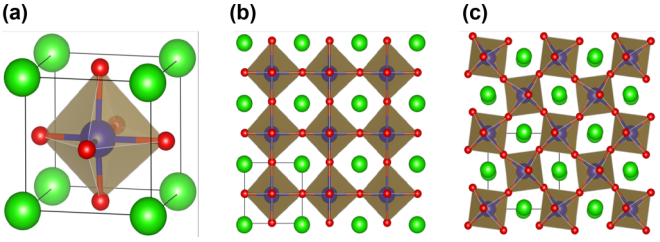

FIG. 1. (a) TaO_6 octahedron in cubic perovskites, (b) c-NTO, and (c) o-NTO crystal structures (side views). Na, Ta, and O are represented with green, blue, and red balls, respectively.

III. RESULTS AND DISCUSSION

A. Bulk properties

The primitive structure of cubic perovskite is shown in Fig. 1, where Ta is octahedrally coordinated to six O atoms [Fig. 1(a)] and Na/K cations sit in the cages of the Ta-O framework [Fig. 1(b)]. Depending on the properties of the cations, e.g., size and electron affinity, a distortion of the octahedra can further stabilize the structure. Using the ionic radii of Na^+ (116 pm), K^+ (152 pm), Ta^{5+} (78 pm), and O^{2-} (126 pm) [37], the computed tolerance factors [$t = \frac{r_A + r_O}{\sqrt{2}(r_B + r_O)}$ for ABO_3 perovskites] of NTO and KTO are 0.839 and 0.964, respectively. The smaller tolerance factor of NTO is consistent with the occurrence of the o-NTO phase, with tilted TaO_6 octahedra [Fig. 1(c)]. The computed (experimental [12,35]) lattice parameters are 3.980 (3.929) and 4.025 (3.988) Å for c-NTO and KTO, respectively; those for o-NTO are 5.590 (5.513), 5.530 (5.494), and 7.858 (7.750) Å. These values agree well with previous DFT studies [21,32], but are overestimated by about 1% in comparison to experiment. Note that the optimized volume of o-NTO is 3.71% smaller with respect to that of c-NTO.

The bonding properties of NTO and KTO are characterized in Table I, where calculated Löwdin charges, cohesive energies, and defect formation energies are reported. Löwdin

TABLE I. Löwdin charges, oxygen vacancy (Vo), and Na/K vacancy (V_A) formation energies (E_{form}, in eV), and cohesive energies (E_{coh}, in eV/f.u.) of c-NTO, o-NTO, and KTO.

		c-NTO	o-NTO	KTO
Löwdin charges	Na/K	0.94	0.92	0.68
	Ta	0.69	0.74	0.87
	O	–0.51	–0.52	–0.48
E_{form}	V_O	5.00	6.19	6.01
	V_A	4.03	5.12	4.61
E_{coh}		32.51	32.58	32.20

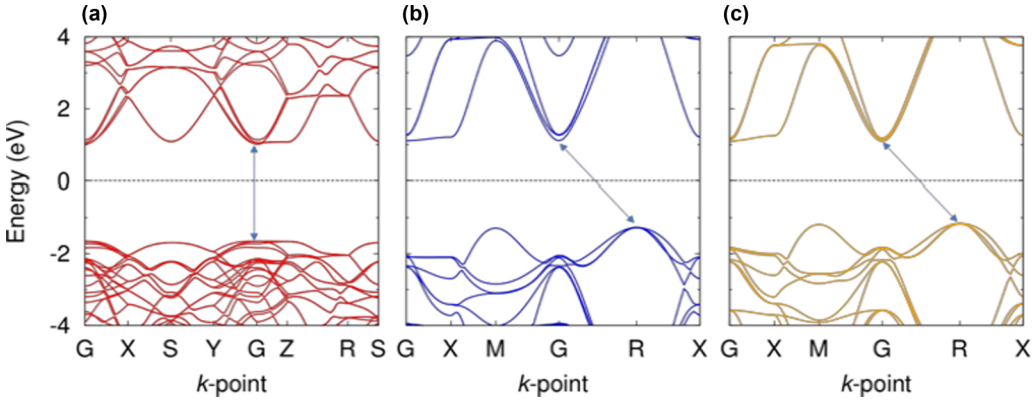

FIG. 2. Computed PBE band structures of (a) o-NTO, (b) c-NTO, and (c) KTO. Comparison to hybrid HSE06 calculations is reported in Fig. S2 in the Supplemental Material [38].

charges indicate a stronger ionicity in NTO with respect to KTO, a finding confirmed by the charge density plots in Fig. S1 of the Supplemental Material (SM) [38]. While differences between c-NTO and o-NTO are small in comparison to those between c-NTO and KTO, we also notice that Ta has a slightly larger positive charge in o-NTO than in c-NTO, suggesting somewhat stronger Ta-O interactions in o-NTO. The cohesive energy of o-NTO is indeed 0.07 eV larger than in c-NTO, while KTO has the smallest cohesive energy, indicating that K^+ ions have a weaker interaction with the TaO_2 framework than Na^+. The oxygen vacancy (Vo) formation energy is 5.00 eV for c-NTO, in agreement with a previous DFT study [31], 6.19 eV for o-NTO, and 6.01 eV for KTO. In c-NTO, Vo formation triggers a local tilting of the TaO_6 octahedra, significantly reducing the formation energy in comparison to o-NTO and KTO.

The band structures of the two phases of NTO and KTO are displayed in Fig. 2. In line with existing reports [11,39], c-NTO shows an indirect band gap while the orthorhombic phase has a direct gap at the Γ point. The band structure of KTO is very similar to that of c-NTO. The results in Fig. 2 were obtained using the PBE functional, which is well known to underestimate band gaps. HSE06 hybrid functional calculations predict larger values of the band gap, but do not change their indirect/direct character (see Fig. S2 in the Supplemental Material [38]). The indirect band gap of c-NTO has been suggested to be a possible contribution to its higher photocatalytic activity relative to the o-NTO phase [11,12], due to the lower recombination rate of electrons and holes in systems with an indirect band gap.

B. Surface energy

The surface energy describes how much (free) energy per unit area is needed to cleave a crystal and expose the resulting surfaces to vacuum. This quantity plays an important role in the synthesis of nanomaterials because it determines which facets are preferentially exposed and thus the shape of the nanoparticles [40], the surface morphology [41], and the reactivity [42,43]. For NTO and KTO, cubiclike particles are typically observed in experiments [44–46], indicating that the polar (001) surface is preferred.

For symmetric and stoichiometric slab models, the surface energy can be simply calculated as

$$\gamma = (E_{\text{slab}} - nE_{\text{bulk}})/2A,$$

where E_{slab} is the total energy of the slab, E_{bulk} is the total energy per formula unit of bulk NTO or KTO, n is the number of formula units in the slab, and $2A$ is the total exposed surface area. For perovskite (001) surfaces, however, this expression is not directly applicable because symmetric slab models are nonstoichiometric whereas stoichiometric models expose both NaO/KO and TaO_2 terminations [Figs. 3(a) and 3(b)]. Instead, we followed the method introduced by Eglitis and Vanderbilt [47] based on stoichiometric slab models. First, we calculate the surface energy of the as-cleaved slab as

$$\gamma_0 = (E_{\text{slab0}} - nE_{\text{bulk}})/(2A),$$

where E_{slab0} is the total energy of the as-cleaved (unrelaxed) slab and A is the surface area of each side. γ_0 represents the energy per unit area that is required to break the bonds between the two terminations. Next, we relax the atomic

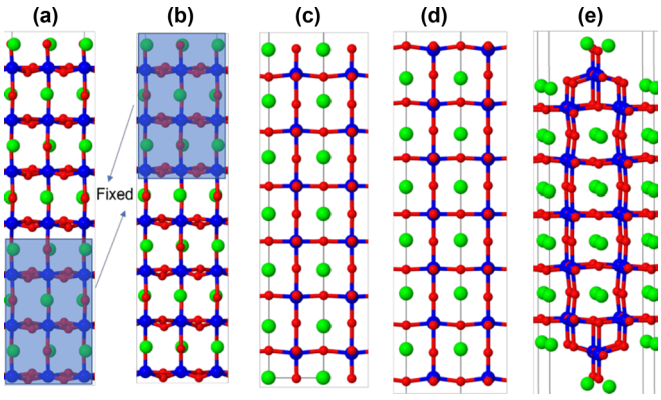

FIG. 3. Some of the c-NTO (001) slab models considered in the present work: (a,b) Nonsymmetric stoichiometric slab; (c) NaO-terminated symmetric nonstoichiometric slab; (d) TaO_2-terminated symmetric nonstoichiometric slab; (e) (2×2) cation-exchange reconstruction. Sodium, tantalum, and oxygen are represented with green, blue, and red balls, respectively. The shaded blue areas in (a,b) indicate the layers that are kept frozen in the calculation of surface energies.

TABLE II. Surface energies ($J\,m^{-2}$) for different surface structures/terminations of c-NTO, o-NTO, and KTO (001). Results for the striped surface with coexisting NaO/KO and TaO_2 terminations refer to a slab model with $w = 3$; surface energies for different w values are presented in Fig. S3 in the Supplemental Material [38].

Surface structure/termination	c-NTO	o-NTO	KTO
TaO_2	1.20	1.18	1.05
NaO/KO	1.65	1.64	1.46
Striped	0.89	1.17	0.75
Cation exchange	0.75	0.88	0.68

positions of only one half of the slab, while keeping the other half fixed. This gives the relaxation energy $E_{\rm relax} = E_{\rm slab} - E_{\rm slab0}$, which is normalized by surface area and added to γ_0 to obtain an approximate estimate of the surface energy:

$$\gamma = \gamma_0 + E_{\rm relax}/A.$$

This procedure was applied successively to the two different halves of each slab and tested for convergence with respect to the number of layers in the slab. Our results for the two separate terminations of c-NTO, o-NTO, and KTO are reported in Table II. We can see that for all of the three investigated perovskites, the surface energy is more than $0.4\,J\,m^{-2}$ lower for the TaO_2 termination than for the NaO/KO one. This indicates that the TaO_2 termination, exposing the less ionic Ta-O bonds, releases more energy through relaxation than the NaO/KO one. In comparison to the two phases of NTO, KTO has significantly lower surface energy for both the KO and TaO_2 terminations, consistent with the lower cohesive energy of KTO.

C. Coexisting NaO/KO and TaO_2 terminations vs cation-exchange reconstruction

The coexistence of two different terminations is a compensating mechanism that is frequently observed on the polar surfaces of transition metal oxides; for example, it has been reported for Fe_2O_3 [19,20] and ZnO [48,49]. We investigated this mechanism for NTO(001) and KTO(001), using surface models where the two terminations form terraces of equal width separated by monoatomic steps along the [110] direction, as recently reported for KTO(001) [21]. The optimized structures of such models for c-NTO, o-NTO, and KTO (001) are shown in Fig. 4 for the case of terrace width $w = 3$. We can notice some differences in the structure of the relaxed outer layers on the KTO and NTO surfaces, which can be largely attributed to the different radii of Na^+ and K^+: While on KTO (001) the outer layer does not show significant structural changes, on NTO (001) the topmost NaO terrace tends to contract laterally, becoming more compact. Moreover, Na^+ cations beneath the TaO_2 terrace relax inward (i.e., away from the surface toward the bulk), suggesting an effective positive charge on the TaO_2 terrace. Oxygen atoms on the exposed TaO_2 terrace tend to displace outward, while oxygen atoms beneath the outer NaO/KO terrace displace inward.

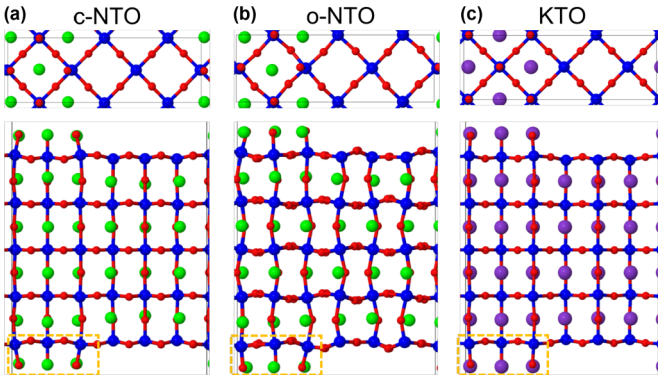

FIG. 4. Top (above) and side (below) views of surface models with coexisting TaO_2 and NaO/KO-terminated terraces of width $w = 3$ on (a) c-NTO (001), (b) o-NTO (001), and (c) KTO (001). Sodium, potassium, tantalum, and oxygen are represented with green, purple, blue, and red balls, respectively. The rectangle (orange dashed lines) on the bottom surface of each slab highlights the lateral contraction of the outermost NaO/KO layer, which is more pronounced for NaO than for KO.

The surface energies of coexisting NaO/KO and TaO_2 terraces were calculated using stoichiometric and symmetric slab models (Fig. 4). Results are reported in Table II (case $w = 3$) and Fig. S3 in the Supplemental Material [38]. As shown in the latter figure, while the computed dependence of the surface energy on the terrace width is stronger for NTO phases than for KTO, $w = 3, 4$ is slightly preferred for both NTO and KTO. From Table II, we can further see that the surface with mixed terminations is only $0.01\,J\,m^{-2}$ more stable than the pure TaO_2 termination for o-NTO, while it is as much as $\sim 0.3\,J\,m^{-2}$ more stable than the pure TaO_2 termination for both c-NTO and KTO.

Surface stress is known to play an important role in driving surface reconstructions [50]. Hence, it is interesting to investigate its relevance in the stability of the striped phases on KTO and c-NTO. To evaluate the surface stress, we used the symmetric slab models in Figs. 3(c) and 3(d) and for each termination determined the total energy of the slab for different values of the lattice parameter along [100]. Figure 5 shows that the TaO_2 terminations of both c-NTO and KTO would prefer to contract, i.e., are under tensile stress. This is not surprising considering the partially covalent character of the Ta-O bonds and the reduced atomic coordination at the surface. Similar to the TaO_2 termination, the extended NaO termination is under tensile stress, while the KO termination is essentially at its optimal lattice constant. This behavior is consistent with the different sizes of the Na^+ and K^+ ions and the structures in Fig. 4. Explicit values of the surface stress, computed from $\frac{\Delta E}{2A\Delta\varepsilon}|_{\Delta\varepsilon=0}$ [51], are 4.40 and $2.73\,J/m^2$ for the NO and TO terminations of c-NTO, vs 0.06 and $5.37\,J/m^2$ for the KO and TO terminations of KTO. Altogether, these results suggest that formation of finite size domains of exposed NaO/KO and TaO_2 can reduce the surface stress, thus contributing to the higher stability of the striped phase relative to the pure TaO_2 termination on both KTO and c-NTO (Table II).

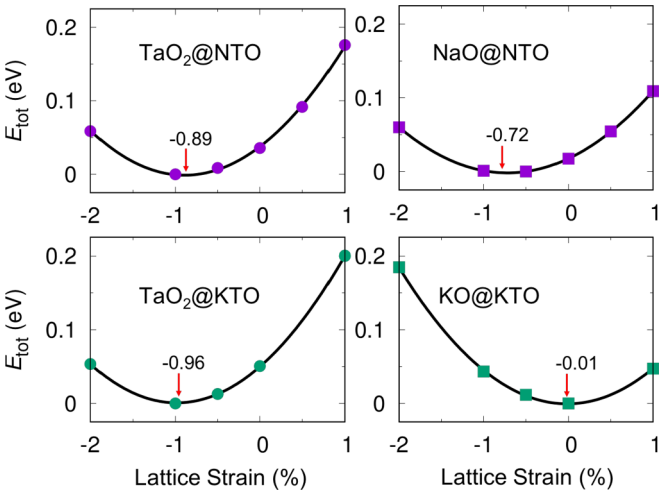

FIG. 5. Total energy vs lattice strain (%) along [100] for the symmetric c-NTO (001) (upper panels) and KTO (001) (lower panels) slab models in Figs. 3(c) and 3(d). The minimum of each curve and the corresponding value of the abscissa are reported. Label example: TaO_2@NTO indicates the TaO_2 termination of a $NaTaO_3$ slab.

1. Cation-exchange reconstruction

The cation-exchange mechanism [18] was originally identified using a global optimization procedure on a $p(2 \times 2)$ slab model [see Fig. 3(e)] that is not compatible with the striped structure discussed above. As shown in Table II, the cation-exchange reconstruction is only slightly more favorable, $0.07\,\mathrm{J\,m^{-2}}$, than the striped phase for KTO (001). The fact that striped phases are actually observed in experiment may be thus an indication of a high kinetic barrier for the cation-exchange reconstruction on this surface. In contrast, the cation-exchange reconstruction is 0.14 and $0.29\,\mathrm{J\,m^{-2}}$ more favorable than the striped surface for c-NTO (001) and o-NTO (001), respectively, suggesting that NTO is more likely to undergo such surface reconstructions rather than forming a striped phase.

D. Electronic structure

1. Pure NaO/KO and TaO_2 terminations

Our results for the single NaO/KO and TaO_2 terminations of c-NTO and KTO (001) are summarized in Fig. 6, which shows layer-resolved densities of states (LRDOS) for two types of models: asymmetric stoichiometric slabs and slabs supported on a metal (tantalum) substrate, as are often present in experiments [35,36]. The slabs are 7 or 6.5 layers thick (here "layer" indicates a unit cell, i.e., two atomic layers), corresponding to 14 or 13 atomic layers.

While for thick films of a polar material compensation occurs naturally, the polarity can remain uncompensated in the case of a thin film [17]. This is evident from the LRDOS for the nonsymmetric slabs in the upper part of Fig. 6, which show an electrostatic potential energy drop (as indicated by the shift of the band edges) between the two sides of the slab. It also appears that the potential drop is smaller in the NTO (left) than in the KTO (right) slab, so that the overall band gap is larger in NTO than in KTO. As shown by the corresponding optimized structures, in each atomic layer the Ta/Na/K cations and O anions shift in opposite directions in order to compensate the polarity. The relative displacements, Δz, of cations and anions in the direction perpendicular to the surface are listed in Table III. Δz is in the range of 0.20–0.27 Å for the TaO_2 sublayers of both NTO and KTO, it is 0.15–0.21 Å for the KO sublayers of KTO, and it is typically twice the latter values for the NaO sublayers of NTO (an exception is the first NaO sublayer, where Δz has opposite sign with respect to all other sublayers to let the oxygens protrude outside the surface more than the Na^+). Altogether, it is apparent that, compared to K^+, the smaller Na^+ ions respond much more effectively to compensate the polarity of the system.

To make closer contact with experimental studies where NTO is often grown on a Ta metal substrate [35,36], we have also computed the electronic structure of both NaO/KO- and TaO_2-terminated NTO and KTO slabs on top of a metallic Ta slab (denoted NTO/Ta and KTO/Ta, respectively). We assumed the contact layer to the Ta metal to be TaO_2; NaO/KO contact layers were not considered after test calculations on simple structural models showed strong structural rearrangements, suggesting the necessity of more refined models of the interface. For the NaO/KO-terminated stoichiometric slabs (middle panels of Fig. 6), the presence of the metal substrate reduces the dipole field in the slab. Again, the polarity compensation is more effective in NTO/Ta, where the valence band maximum edge varies by only 0.65 eV, than for the KTO/Ta slab, for which the energy drop is 1.20 eV. The TaO_2-terminated slabs (bottom part of Fig. 6) are nonstoichiometric and electron rich.

For comparison, the layer-resolved DOS of the fully compensated (2×2) cation-exchanged NTO and KTO (001) surfaces have been also calculated; see Fig. S4 in the Supplemental Material [38]. An interesting feature is that the band gap of the surface layer is much wider than the gap of the inner bulklike layers, which reflects the high stability of this surface reconstruction.

2. Coexisting NaO/KO and TaO_2 terminations

We have determined the electronic structure of NTO and KTO surfaces with coexisting terminations for different values $w = 2, 3, 4, 5$ of the width of the terraces. Since differences among the different widths are seen mostly in the densities of states of the outer NaO/KO and TaO_2 terraces, only the latter are reported in Fig. 7.

The general trend is that as the terraces become increasingly wider, the partial DOS of the NaO/KO sublayer in the valence band tends to shift upward with respect to the occupied partial DOS of the TaO_2 sublayer. This shift suggests that, as the width of the stripes increases, the NaO/KO regions accommodate more negative charge, which increases the energy of the electrons therein. As a result, the total DOS and band gap become more similar to those of the extended surfaces in Fig. 6. In particular, the band edges become spatially separated, with KO/NaO terraces contributing to the valence band edge, and TaO_2 terraces contributing to the conduction band edge. For KTO and c-NTO, the separation is observed for $w \geqslant 5$, in good agreement with Ref. [21], while for o-NTO separation seems to require even wider steps.

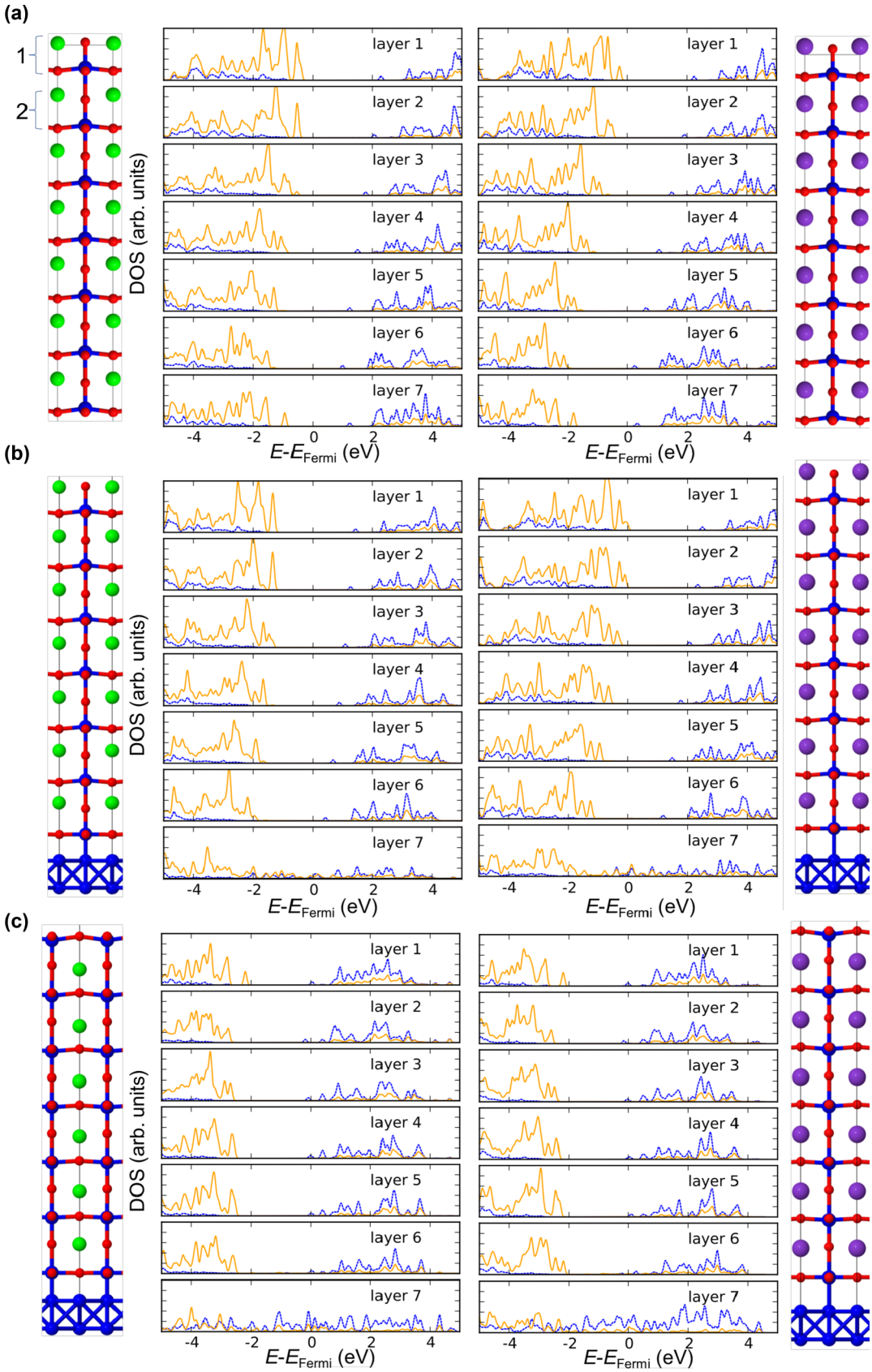

FIG. 6. Layer-resolved density of states for NTO(001) (left) and KTO(001) (right) computed using different slab models. Orange and blue lines represent the NaO/KO and TaO_2 partial DOS, respectively. Top: asymmetric stoichiometric slab; middle: asymmetric stoichiometric slab on Ta metal substrate; bottom: symmetric TaO_2-terminated slab on Ta metal substrate. Na, K, Ta, and O are represented with green, purple, blue, and red balls, respectively.

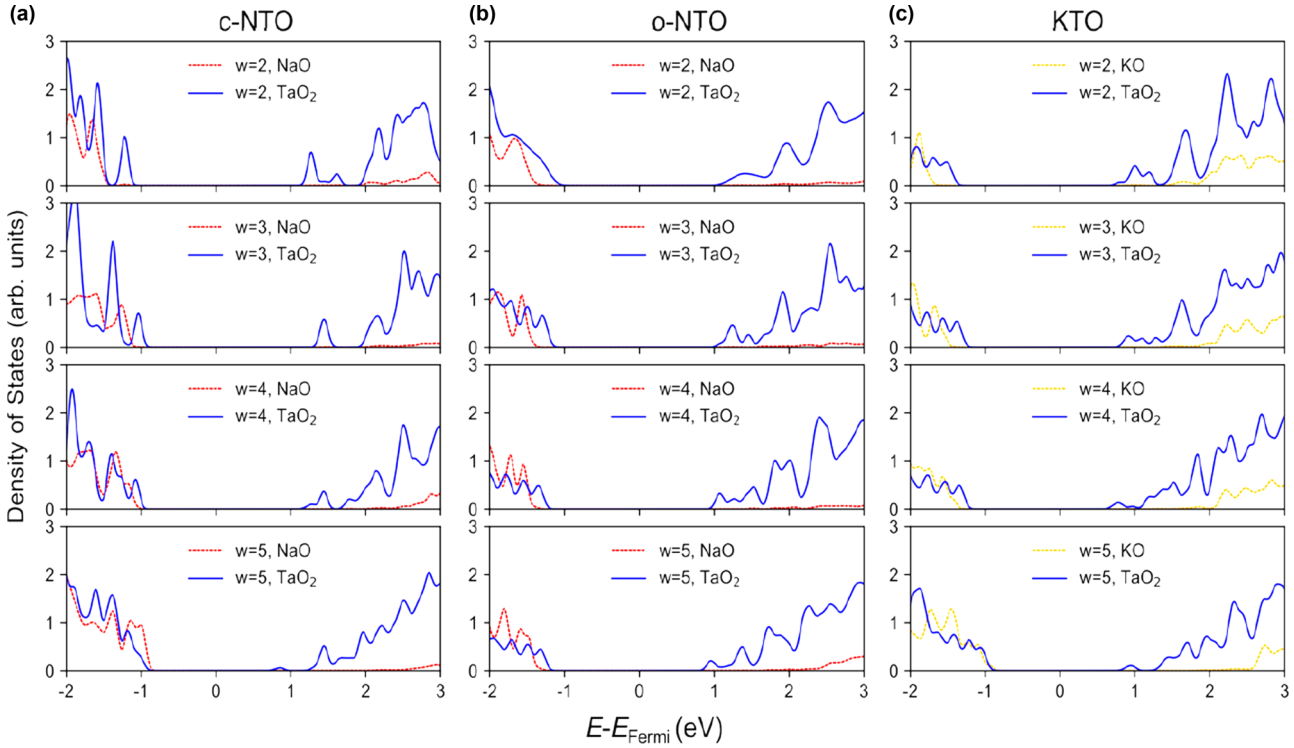

FIG. 7. Density of states of the topmost NaO/KO and TaO_2 atomic layers of c-NTO, o-NTO, and KTO as a function of the terrace width $w = 2, 3, 4, 5$. Red, orange, and blue curves refer to NaO, KTO, and TaO_2, respectively.

E. Interaction with water

To investigate the effect of water adsorption on c-NTO (001) and KTO (001), we considered the three different structural models shown in Fig. 8, namely: the (2×1) hydroxylated surface model, which is based on both DFT calculations and experimental observations [21]; a structure obtained by adsorbing water molecules onto the cation exchange model of Ref. [18]; and finally water adsorbed on the striped surface with terrace width $w = 2$. All the models are stoichiometric

TABLE III. Relative displacements (Å) of cations (Ta or Na/K) and anions (O) along the [001] direction in asymmetric stoichiometric c-NTO(001) and KTO(001) slabs. Layers are defined as in Fig. 6.

	Sublayer	c-NTO	KTO
Layer 1	NaO/KO	–0.07	0.18
	TaO_2	0.22	0.20
Layer 2	NaO/KO	0.35	0.21
	TaO_2	0.21	0.20
Layer 3	NaO/KO	0.40	0.20
	TaO_2	0.21	0.20
Layer 4	NaO/KO	0.40	0.20
	TaO_2	0.21	0.20
Layer 5	NaO/KO	0.40	0.21
	TaO_2	0.22	0.20
Layer 6	NaO/KO	0.39	0.20
	TaO_2	0.22	0.21
Layer 7	NaO/KO	0.29	0.15
	TaO_2	0.27	0.26

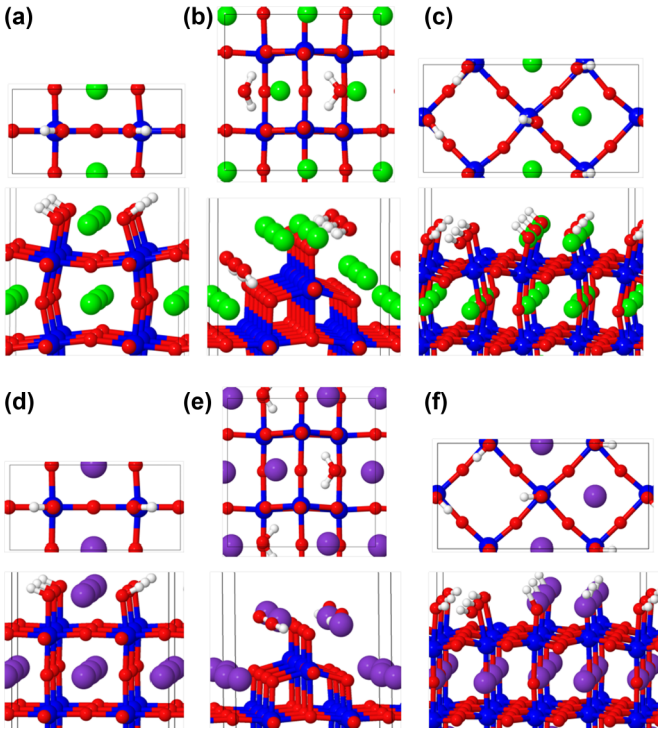

FIG. 8. Top (above) and side (below) views of different structural models of adsorbed water on (a–c) c-NTO (001), and (d–f) KTO (001). (a,d): Hydroxylated $r(2 \times 1)$ model proposed in Ref. [21]. (b,e) Water adsorbed on the $r(2 \times 2)$ reconstructed surface of Ref. [18]. (c,f) Water adsorbed on the $(2\sqrt{2} \times \sqrt{2})$ striped surface (terrace width $w = 2$).

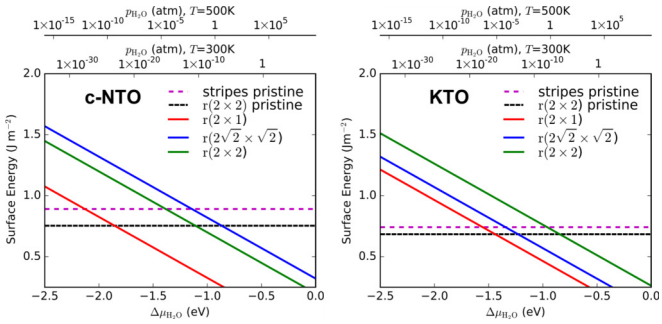

FIG. 9. Surface phase diagram of c-NTO (left) and KTO (right) in contact with water vapor. Here "stripes pristine" refers to the striped surface models in Fig. 4; "$r(2 \times 2)$ pristine" is the cation-exchange reconstruction; $r(2 \times 1)$, $r(2 \times 2)$, and $r(2\sqrt{2} \times \sqrt{2})$ are the water adsorption models in Fig. 8, panels (a,d), (b e), and (c,f), respectively.

and the water coverage is 0.5 monolayer (ML), referring to the number of Ta atoms in the layer.

Compared to KTO, whose -Ta-O- framework shows little distortion, adsorption of water generally introduces significant distortion of the octahedra in c-NTO. For example, one can notice that the water adsorption on the $r(2 \times 2)$ reconstructed NTO surface induces the displacement of a sodium cation, confirming the greater flexibility of the NTO surface relative to KTO. As a consequence, more energy can be released through water adsorption on NTO than on KTO.

Our results for the surface stability in a humid environment are summarized in Fig. 9, which shows the formation energies of several structural models of both clean and water covered c-NTO and KTO (001) as a function of the water chemical potential. While the $r(2 \times 2)$ cation-exchange reconstruction is the preferred structure at low water pressure, upon water adsorption a hydroxylated (2×1) surface is the most stable structure in a wide range of water chemical potential. The layer-resolved DOS of the hydroxylated $r(2 \times 1)$ structure is reported in Fig. S5 in the Supplemental Material [38].

IV. CONCLUSIONS

We have presented first-principles slab calculations aimed at understanding the structure and energetics of the polar (001) surfaces of monoclinic and orthorhombic $NaTaO_3$ (c-NTO and o-NTO) and cubic $KTaO_3$ (KTO), three perovskite oxides of considerable interest in photocatalysis and related applications. Among several investigated structures—pure NaO/KO and TaO_2 terminations, alternating stripes of equally exposed NaO/KO and TaO_2 terminations, cation-exchange reconstruction, and surface with an overlayer of adsorbed water—the cation-exchange reconstruction is found to be energetically preferred on all investigated surfaces under vacuum conditions. For KTO (001), this reconstruction is even slightly more stable than the experimentally observed striped structure, suggesting that kinetic effects are important in determining the actual surface stabilization mechanism. For NTO, the stability of the cation-exchange structure is significantly more pronounced than for KTO, suggesting that the striped structure is unlikely to form on this material, especially on the o-NTO phase. Our results show that, due to the smaller size of the Na^+ cation relative to K^+, NTO exhibits enhanced structural flexibility and more effective charge compensation in comparison to KTO. Moreover, although c-NTO is less stable than o-NTO in the bulk phase, c-NTO (001) has lower surface energy than o-NTO (001), consistent with the experimental observation of higher specific surface area of c-NTO. For all investigated materials, a (2×1) hydroxylated structure, where Ta ions at TaO_2 terraces are stabilized through interaction with the oxygens of water [Figs. 8(a) and 8(d)], becomes far more favorable upon water adsorption. Due to its high stability, this (2×1) hydroxylated structure is likely to be present also under conditions relevant to photocatalytic water splitting, thus providing a basis for the mechanistic understanding of photocatalytic processes on NTO surfaces.

ACKNOWLEDGMENTS

This work was supported by DoE-BES, Division of Chemical Sciences, Geosciences and Biosciences under Award No. DE-SC0007347. We used resources of the National Energy Research Scientific Computing Center (DoE Contract No. DE-AC02-05CH11231). We also acknowledge use of the TIGRESS high-performance computer center at Princeton University.

[1] H. Kato and A. Kudo, Chem. Phys. Lett. **295**, 487 (1998).
[2] H. Kato, K. Asakura, and A. Kudo, J. Am. Chem. Soc. **125**, 3082 (2003).
[3] G. Zhang, G. Liu, L. Wang, and J. T. S. Irvine, Chem. Soc. Rev. **45**, 5951 (2016).
[4] M. Kubicek, A. H. Bork, and J. L. M. Rupp, J. Mater. Chem. A **5**, 11983 (2017).
[5] I. Grinberg *et al.*, Nature **503**, 509 (2013).
[6] A. Pérez-Tomás, A. Mingorance, D. Tanenbaum, and M. Lira-Cantú, *The Future of Semiconductor Oxides in Next-Generation Solar Cells* (Elsevier, Amsterdam, 2018).
[7] S. Mathews, R. Ramesh, T. Venkatesan, and J. Benedetto, Science **276**, 238 (1997).
[8] J. S. Manser, J. A. Christians, and P. V. Kamat, Chem. Rev. **116**, 12956 (2016).
[9] P. Zhang, J. Zhang, and J. Gong, Chem. Soc. Rev. **43**, 4395 (2014).
[10] E. Grabowska, Appl. Catal., B **186**, 97 (2016).
[11] W.-H. Lin, C. Cheng, C.-C. Hu, and H. Teng, Appl. Phys. Lett. **89**, 211904 (2006).
[12] C.-C. Hu, C.-C. Tsai, and H. Teng, J. Am. Ceram. Soc. **92**, 460 (2009).
[13] C.-C. Hu and H. Teng, Appl. Catal., A **331**, 44 (2007).
[14] P. D. C. King, R. H. He, T. Eknapakul, P. Buaphet, S.-K. Mo, Y. Kaneko, S. Harashima, Y. Hikita, M. S. Bahramy, C. Bell, Z. Hussain, Y. Tokura, Z.-X. Shen, H. Y. Hwang, F. Baumberger, and W. Meevasana, Phys. Rev. Lett. **108**, 117602 (2012).
[15] P. W. Tasker, J. Phys. C: Solid State Phys. **12**, 4977 (1979).
[16] C. Noguera, J. Phys.: Condens. Matter **12**, R367 (2000).
[17] C. Noguera and J. Goniakowski, Chem. Rev. **113**, 4073 (2013).

[18] D. E. E. Deacon-Smith, D. O. Scanlon, C. R. A. Catlow, A. A. Sokol, and S. M. Woodley, Adv. Mater. **26**, 7252 (2014).
[19] A. Kiejna and T. Pabisiak, J. Phys. Chem. C **117**, 24339 (2013).
[20] M. Lewandowski *et al.*, Chem. Mater. **28**, 7433 (2016).
[21] M. Setvin, M. Reticcioli, F. Poelzleitner, J. Hulva, M. Schmid, L. A. Boatner, C. Franchini, and U. Diebold, Science **359**, 572 (2018).
[22] L. An, T. Sasaki, P. G. Weidler, C. Wöll, N. Ichikuni, and H. Onishi, ACS Catal. **8**, 880 (2018).
[23] L. M. Feng, L. Q. Jiang, M. Zhu, H. B. Liu, X. Zhou, and C. H. Li, J. Phys. Chem. Solids **69**, 967 (2008).
[24] Q. Sun and W.-J. Yin, J. Am. Chem. Soc. **139**, 14905 (2017).
[25] P. Giannozzi *et al.*, J. Phys.: Condens. Matter **21**, 395502 (2009).
[26] J. P. Perdew, K. Burke, and M. Ernzerhof, Phys. Rev. Lett. **77**, 3865 (1996).
[27] D. Vanderbilt, Phys. Rev. B **41**, 7892 (1990).
[28] G. Prandini, A. Marrazzo, I. E. Castelli, N. Mounet, and N. Marzari, npj Comput. Mater. **4**, 72 (2018).
[29] V. Blum, R. Gehrke, F. Hanke, P. Havu, V. Havu, X. Ren, K. Reuter, and M. Scheffler, Comput. Phys. Commun. **180**, 2175 (2009).
[30] S. V. Levchenko, X. Ren, J. Wieferink, R. Johanni, P. Rinke, V. Blum, and M. Scheffler, Comput. Phys. Commun. **192**, 60 (2015).
[31] M. Choi, F. Oba, and I. Tanaka, Phys. Rev. B **78**, 014115 (2008).
[32] X. Liu and K. Sohlberg, Comput. Mater. Sci. **103**, 1 (2015).
[33] H. J. Monkhorst and J. D. Pack, Phys. Rev. B **13**, 5188 (1976).
[34] L. Bengtsson, Phys. Rev. B **59**, 12301 (1999).
[35] S. Suzuki, K. Teshima, K. Yubuta, S. Ito, Y. Moriya, T. Takata, T. Shishido, K. Domen, and S. Oishi, CrystEngComm **14**, 7178 (2012).
[36] Y. Lee, T. Watanabe, T. Takata, J. N. Kondo, M. Hara, M. Yoshimura, and K. Domen, Chem. Mater. **17**, 2422 (2005).
[37] R. Shannon, Acta Crystallogr., Sect. A **32**, 751 (1976).
[38] See Supplemental Material at http://link.aps.org/supplemental/10.1103/PhysRevMaterials.3.015801 for electron density distributions, HSE06 bulk band structures, surface energies as a function of stripe width, and layer-resolved DOS of (2 × 2) cation-exchanged and (2 × 1) hydroxylated c-NTO and KTO (001) surfaces.
[39] X. Liu and K. Sohlberg, Comput. Mater. Sci. **123**, 1 (2016).
[40] A. S. Barnard and L. A. Curtiss, Nano Lett. **5**, 1261 (2005).
[41] S. Selcuk, X. Zhao, and A. Selloni, Nat. Mater. **17**, 923 (2018).
[42] X. Xie, Y. Li, Z.-Q. Liu, M. Haruta, and W. Shen, Nature **458**, 746 (2009).
[43] S. Selcuk and A. Selloni, Nat. Mater. **15**, 1107 (2016).
[44] L. Polak, J. H. Rector, M. J. Slaman, and R. J. Wijngaarden, J. Phys. Chem. C **120**, 23559 (2016).
[45] Q. Zhang, Z. Li, S. Wang, R. Li, X. Zhang, Z. Liang, H. Han, S. Liao, and C. Li, ACS Catal. **6**, 2182 (2016).
[46] B. Bajorowicz, A. Cybula, J. M. Winiarski, T. Klimczuk, and A. Zaleska, Molecules **19**, 15339 (2014).
[47] R. I. Eglitis and D. Vanderbilt, Phys. Rev. B **76**, 155439 (2007).
[48] G. Kresse, O. Dulub, and U. Diebold, Phys. Rev. B **68**, 245409 (2003).
[49] D. Mora-Fonz, T. Lazauskas, M. R. Farrow, C. R. A. Catlow, S. M. Woodley, and A. A. Sokol, Chem. Mater. **29**, 5306 (2017).
[50] O. L. Alerhand, D. Vanderbilt, R. D. Meade, and J. D. Joannopoulos, Phys. Rev. Lett. **61**, 1973 (1988).
[51] J. Harl and G. Kresse, Surf. Sci. **600**, 4633 (2006).